RSC Advances

PAPER

View Article Online
View Journal | View Issue

Cite this: *RSC Adv.*, 2025, **15**, 2224

Study on the Brill transition of polyamide 6 with different crystal forms using low- and high-frequency Raman spectroscopy†

Jiacheng Gao and Harumi Sato *

Received 3rd December 2024
Accepted 14th January 2025

DOI: 10.1039/d4ra08523j

rsc.li/rsc-advances

Polyamide 6 (PA6) in its α and γ-forms was studied from 30 to 220 °C using Raman spectroscopy in the low- and high-wavenumber regions. Quantum chemical calculations were employed to assist with band assignments. In the low-wavenumber region, a peak at approximately 100 cm^{-1}, attributable to a mixed mode of methylene lateral motion and amide group stretching, was observed. Additionally, a new band at approximately 60 cm^{-1} was observed and assigned to molecular chain torsions in the α-form. Both bands indicated that molecular chain rotation occurs prior to the Brill transition at approximately 130 °C. In the high-wavenumber region, bands at approximately 1126 cm^{-1} and 1060 cm^{-1} indicated a simultaneous weakening of C–C stretching modes in the *trans* conformation at the same temperature, consistent with observations in the low-wavenumber region.

Introduction

Polyamide, commonly known by the commercial name nylon, is one of the earliest synthetic plastics invented by humans and remains one of the most widely used polymers in terms of annual production.[1–4] Polyamide 6 (PA6) is valued for its high tensile strength, elasticity, excellent thermal and mechanical properties, and the ability to plasticize by absorbing water,[5,6] allowing it to be widely used in engineering plastics and synthetic fibers.[7,8]

PA6 has two main crystalline phases: the α and γ-forms that are differentiated based on the orientations of the molecular chains and hydrogen bonding.[9,10] Additionally, the γ-form is relatively unstable.[11] Hydrogen bond formation also results in interesting and unique properties, such as the Brill transition. The crystalline structure of PA6 changes from monoclinic to pseudo-hexagonal[12] upon reaching a specific temperature near 160 °C.[13] It has been suggested that the formation of pseudo-hexagonal structures originates from torsion in the backbone and rearrangement of hydrogen bonds.[14–16]

In the past, polyamides have been studied using various spectroscopic and non-spectroscopic methods. Using X-ray diffraction techniques, infrared (IR) spectroscopy, terahertz spectroscopy, and Raman spectroscopy, researchers have investigated the crystallinity and microstructure of polyamides,[17–19] as well as the thermal degradation and weathering,[20–22] thermal and mechanical behavior,[23–25] and water absorption and moisture content[26–29] of polyamides and their composite materials.

Although as early as 1998, Vasanthan *et al.*[30] reported that the integrated IR band at 1224 cm^{-1} in PA6,6, and bands at 1292 cm^{-1} and 1213 cm^{-1} in PA6 decrease and disappear completely at the Brill transition point, spectroscopic studies on the Brill transition of various polyamides remain relatively limited and serve mostly as a complement to X-ray methods.[31–36] In 2013 and 2015, Suzuki *et al.*[9,10] reported that the bands at 8.7 THz and 6.5 THz in the terahertz absorption spectra were associated with the glass transition and Brill transition, respectively. In addition, they observed an anomaly at approximately 110 °C in the bands at 6.5 THz and 1.75 THz in amorphous PA6. In 2016 and 2018, Musso *et al.* and Menezes *et al.*[12,37] conducted Raman spectroscopic investigations on the Brill transition of PA6,6 and confirmed that the bands at 1479 cm^{-1} and 1126 cm^{-1}, assigned to CNH bending and C–C skeletal stretching, respectively, were related to the Brill transition. In addition, they observed that the anti-Stokes/Stokes Raman intensity ratio of the peak at 100 cm^{-1} could be used to identify the Brill transition temperature. In 2019, Yamamoto *et al.*[38] studied low-frequency vibrational modes in PA6 using far-infrared (FIR) and low-frequency Raman spectroscopies, identifying the FIR bands at 222 cm^{-1} and 111 cm^{-1} as characteristic of the α-form structure, attributable to the glass transition and Brill transition, respectively; however, there is still a gap in Raman studies related to the Brill transition of PA6, especially in the low-wavenumber region.

Recently, Raman spectroscopy has become a commonly used analytical tool for researchers in various fields. By examining the wavenumber, position shift, polarization, width, intensity,

Graduate School of Human Development and Environment, Kobe University, 3-11, Tsurukabuto, Nada-ku, Kobe, Hyogo, 657-0011, Japan. E-mail: hsato@tiger.kobe-u.ac.jp

† Electronic supplementary information (ESI) available. See DOI: https://doi.org/10.1039/d4ra08523j

and other parameters of peaks in a Raman spectrum, a wealth of information regarding the composition, tension/stress, crystal symmetry and orientation, crystal mass, amount of matter, *etc.* of a substance can be obtained.[39] Compared with IR spectroscopy, Raman spectroscopy yields similar but complementary data.[40] It has many advantages, such as being noninvasive, requiring almost no sample preparation, the ability to determine trace samples, and much less sensitivity to water molecules.[41]

For a long time, acquiring Raman spectra in the low-wavenumber region has been challenging.[42,43] The Raman scattering signal in the low-frequency region can be flooded by the Rayleigh scattering signal, resulting in steep baselines and poor spectral quality. The long focal length of the triple monochromator used in the past to acquire low-frequency Raman spectra resulted in low photon fluxes and long acquisition times.[44] In the last decade, newer filtering techniques based on Bragg diffraction have become available, allowing ultra-low frequency modes down to 5–10 cm^{-1} for Raman spectroscopy.[43,45]

In addition to the research on PA6 mentioned earlier,[38] utilizing low-frequency Raman spectroscopy, the intermolecular interactions, molecular structures, and crystal transitions in various polymers, such as PHB,[46–48] PGA,[49,50] PCL,[51] PBS,[52] PET,[53,54] PBT,[53,54] and PTT[54] were investigated. The bands in the low-wavenumber region were assigned successfully, with some assignments assisted by quantum chemical calculations.

The purpose of this study is to investigate the behavior of PA6 materials with different crystalline phases during temperature variations. The main method used is low-frequency Raman spectroscopy, with reference from high-frequency Raman spectra in the C–C stretching region and quantum chemical calculations. To the authors' knowledge, this study provides, for the first time, the assignment and analysis of bands of PA6 in Raman spectra below 100 cm^{-1}, considering temperature variations. This approach aims to clarify the Brill transition mechanism in the α-form of PA6 and to fill gaps in Raman spectroscopy research related to PA6.

Experimental section

Materials and sample

We obtained PA6 pellets from Sigma-Aldrich (St. Louis, United States), with a density of 1.084 g mL^{-1}. These pellets exhibit a melting point of 229.5 °C and a glass transition point of 62.5 °C. To create thin films, the PA6 pellets were processed by heating and pressing at 230 °C using an AS ONE AH-2003 pressing machine.

In order to obtain α-form PA6 films, the initial films were placed in a vacuum oven (SANSYO SVD10P), gradually cooled to 160 °C at a rate of −1 °C min^{-1}, and annealed for 16 hours. The resulting films, approximately 100 μm thick, were designated as α-PA6.

For the γ-form PA6 films, a different approach was taken. The initial films were immediately quenched in liquid nitrogen at approximately −196 °C, followed by a 16 hours annealing process in a vacuum oven at 110 °C. The resulting films, approximately 200 μm thick, were named γ-PA6.

Raman spectroscopy

A sample film was placed on a heating stage (LINKAM) and measured using a Raman spectrometer (HORIBA LabRAM HR Evolution) with an excitation laser wavelength of 532 nm. The objective lens was 100× (auto-focus), the acquisition time was 5 seconds, and the accumulation number was 10. The sample was heated from 30 to 220 °C in 10 °C intervals, at a rate of 10 °C min^{-1}, and stabilized for 5 minutes at each step. For the low-wavenumber region, the spectra in 200–10 cm^{-1} were collected through an ultra-low frequency filter with a grating of 600 lines per mm (resolution ≈ 1.5 cm^{-1}) and a laser power of 25 mW. Given the lower relative peak intensities and the limited number of significant figures in the low-wavenumber region, each measurement was performed in triplicate, and the results were averaged. For the high-wavenumber region, the acquisition range was 1700–1000 cm^{-1}, and an edge filter was adopted with a grating of 1800 lines per mm (resolution ≈ 0.5 cm^{-1}) and a laser power of 50 mW. All temperature control and focusing were automatic. For the analyzation, the SPINA (version 3.x24, developed by Yukiteru Katsumoto in the Ozaki Group of Kwansei-Gakuin University) and OriginR (version 6.1054, OriginLab Corporation, Northampton) programs were used.

Quantum chemical calculations

The initial structure of PA6 in the α-form was constructed based on previous studies, which provided molecular coordinates.[55] Given that the lamellar thickness of PA6 is approximately 4.77 nm,[56] corresponding to 2.8 times the length of two monomer units in reverse directions, the chain length was set to three times that value. Based on prior research on computational low-frequency vibrational modes,[38] a unit cell containing nine PA6 chains, as shown in Fig. 1, was set as the target for spectral calculations. Molecular fragments containing two neighboring PA6 chains, each terminated with methyl groups and consisting of two monomer units (Fig. S1†), were generated. The optimal calculations were conducted using Gaussian 09 (ref. 57) with the QGRAD[58] program, employing the CAM-B3LYP[59] functional with an empirical dispersion correction of Grimme's D3 dispersion with Becke–Johnson damping

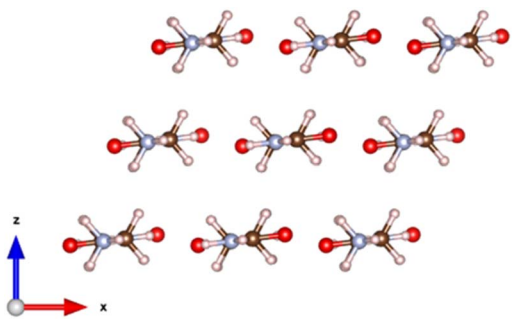

Fig. 1 Unit cell of PA6 in the α-form used in the calculations.

(GD3BJ)[60] and a 6-31++G** basis set. Then, the resultant atomic tensors were transferred back to two neighboring PA6 chains along the *a*-axis at the bottom left corner of the unit cell (Fig. 1) using a Cartesian coordinate tensor transfer (CCT)[61] program. The Avogadro,[62] VESTA,[63] and PLAY[64] programs were utilized for structure building, visualization, and analysis purposes.

Results and discussion

The experimental Raman spectra of a PA6 pellet at room temperature and the corresponding calculated spectra are compared in Fig. 2. The experimental bands at 1126, 1080, 1060, 100, and 60 cm^{-1} can be assigned to the calculated bands at 1160, 1105, 1090, 110, and 70 cm^{-1}, respectively. The Raman shifts of the bands, especially those in the high-wavenumber region, appear blueshifted in the computational spectrum. This is due to the calculations being performed under idealized conditions, assuming a monocrystalline structure without accounting for crystal lattice expansion.[49]

While the newly identified band at approximately 60 cm^{-1} has rarely been mentioned in previous Raman spectroscopic studies, related research in terahertz spectroscopy suggests its connection to a vibration mode along the molecular chain.[9] From Fig. S2,† it can be observed that this band is attributed to motion involving the local rotational movement within the backbone, causing the connected hydrogen atoms to revolve along it.

The band at approximately 100 cm^{-1} appears in several types of polyamides in different papers and has been attributed to a vibration mode related to hydrogen bonds.[65–67] Additionally, a recent computational study suggested that this band correlates with lattice length.[38] Based on the calculated results shown in Fig. S2,† it can be observed that this band is assigned to a motion of backbone carbon atoms vibrating along the *a*-axis with a lateral wagging of hydrogen atoms, accompanied by a stretching motion of N–H and C═O within each molecular chain. As a result, concluding that this band is sensitive to hydrogen bonding and the lattice length is reasonable.

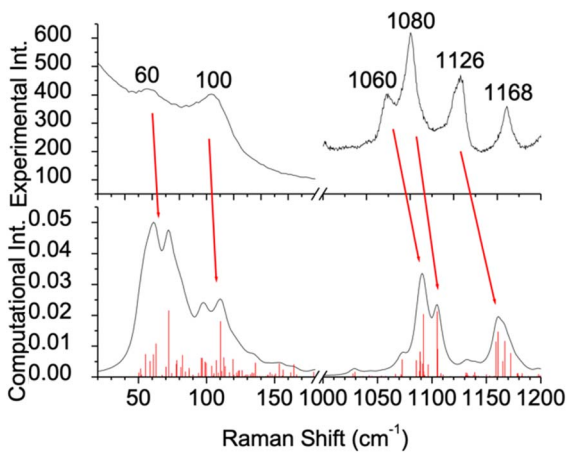

Fig. 2 Comparison and the corresponding relationship of the spectral peaks between the experimental (top) and calculated (bottom) Raman spectra.

The bands at 1060 cm^{-1} and 1126 cm^{-1} are attributable to two different symmetry species of the backbone *trans* C–C stretching vibration,[68] and the band at 1080 cm^{-1} is attributable to the backbone *gauche* C–C stretching vibration.[25] From the corresponding calculational atomic motional modes shown in Fig. S3,† it is evident that the band at 1060 cm^{-1} correlates with strong local C–C stretching motion accompanied by the wagging of hydrogen atoms, whereas the band at 1126 cm^{-1} is associated with overall backbone C–C stretching along with the twisting of hydrogen atoms. Additionally, the band at 1080 cm^{-1} is related to the wagging of hydrogen atoms in directions unparallel to the stretching of carbon atoms, which may be particularly sensitive in a *gauche* conformation.

The temperature-dependent low-frequency Raman spectra of α- and γ-PA6 are shown in Fig. 3(a) and (b), respectively. Due to the effect of Rayleigh scattering near the zero point, the spectra of both samples showed steep baselines and the relative peak intensities decreased with increasing temperature. The spectra of α-PA6 showed two recognizable peaks at approximately 100 and 60 cm^{-1}, while the spectra of γ-PA6 showed only one obvious peak at approximately 100 cm^{-1}. In general, the peaks in the spectra of α-PA6 are clearer than those in the γ-PA6 spectra.

Due to less significant figures and extremely high Rayleigh scattering intensity in the low-wavenumber region, determining the exact peak positions and widths using the second derivative method or curve fitting procedures proved challenging. As a result, a third derivative method was employed to estimate the peak shifts.[69] Additionally, the second derivative intensity was used to represent the peak widths. As previously mentioned, triplicate experiments were performed, and the average values were taken. The processed spectra are displayed in Fig. 3(c)–(f). The Raman shifts and the second derivative intensities of the two peaks at approximately 100 cm^{-1} and 60 cm^{-1} were plotted *versus* temperature for α- and γ-PA6, as shown in Fig. 4.

As shown in Fig. 4(a), the Raman shifts of the bands at approximately 100 cm^{-1} in both samples exhibited a similar trend. They shifted gradually to lower wavenumbers by approximately 5 cm^{-1} as the temperature increased. The plot of the Raman shift showed lower wavenumbers for γ-PA6 compared with α-PA6, despite their similar lattice constants (a_α = 9.56 Å; a_γ = 9.56 Å).[10] As assigned by computational results, this band is associated with hydrogen bonding and lattice length; therefore, the overall redshifts suggest weakening hydrogen bonding due to increased distance between molecular chains. Notably, following the temperature of approximately 160 °C, a slightly accelerated redshift for the band in α-PA6 was observed. This inflection, also reported in previous research on PA6,6,[37] suggests a faster weakening rate of hydrogen bonding after the Brill transition. This aligns with the observation that the transition involves a shift from the α-structure to a γ-like structure.[70,71] On the other hand, the significant reduction in the Raman shift of γ-PA6 at approximately 140 °C suggests that the rearrangement of hydrogen bonding may have slowed the rate of hydrogen bond dissolution in α-PA6. In addition, the

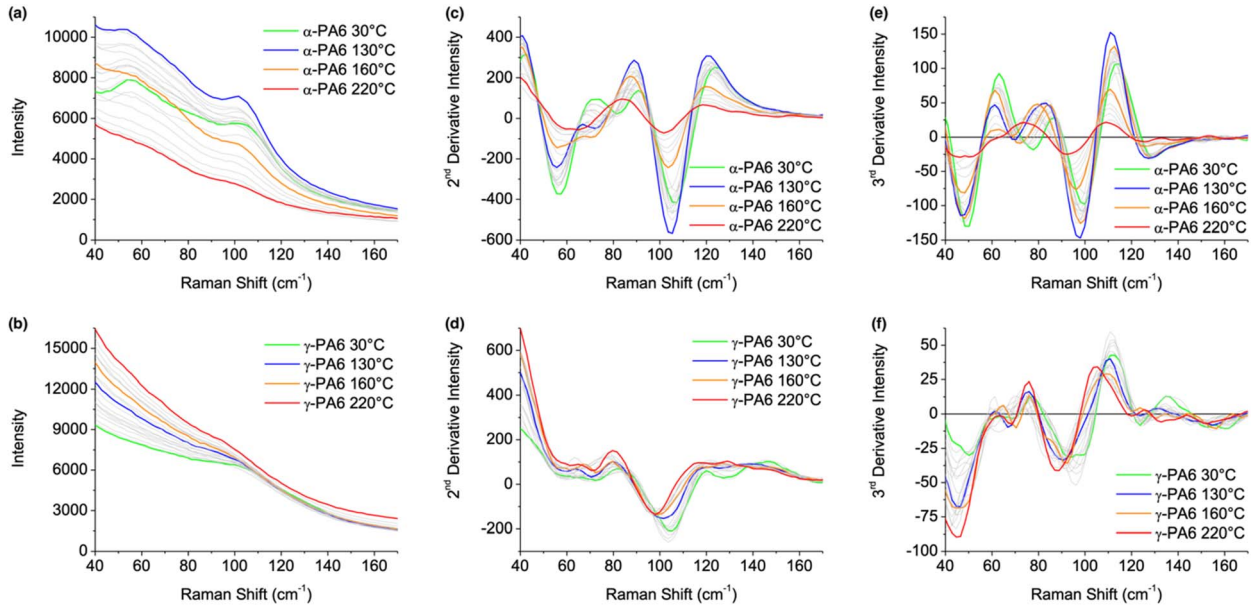

Fig. 3 (a) and (b) Low-frequency Raman spectra of α- and γ-PA6, respectively, (c) and (d) their second derivative spectra, and (e) and (f) their third derivative spectra as a function of temperature from 30 °C to 220 °C.

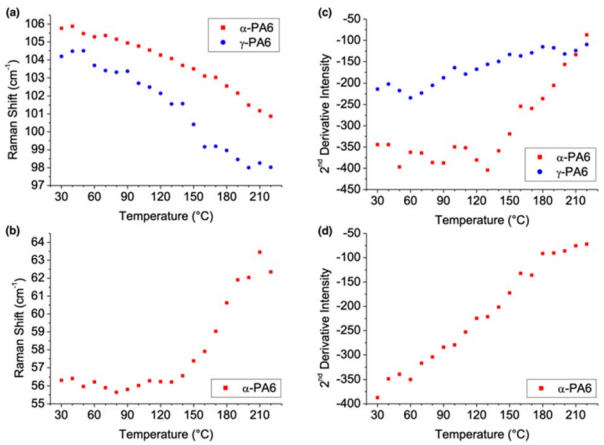

Fig. 4 Raman shift for the bands at approximately (a) 100 cm^{-1} and (b) 60 cm^{-1}, and the second derivative intensities for the bands at approximately (c) 100 cm^{-1} and (d) 60 cm^{-1} as a function of temperature from 30 °C to 220 °C.

band positions beyond 190 °C reflect the differing rates at which these crystal forms reach their melting points, with the γ-form exhibiting a lower melting point.[16]

The Raman shift of the band at approximately 60 cm^{-1} behaved interestingly in α-PA6, as shown in Fig. 4(b). It first remained relatively stable at approximately 56 cm^{-1} before 130 °C and then started to blueshift to approximately 63 cm^{-1}. Suzuki *et al.* reported a similar inflection in the terahertz absorbance spectra at the same wavenumber for amorphous PA6 in earlier research.[10] They suggested that a considerable conformational change likely occurs at this temperature, which, in this study, can be explained by molecular chain rotation, as demonstrated in the computational results. Before the Brill transition, the molecular chains of the α-form were bound *via* hydrogen bonding and methylene conformation, so it was less active, and the molecule was more thermally stable. When heated to approximately 130 °C, the hydrogen bonds between the molecular chains weaken to a certain extent, significantly enhancing the rotational motion of the molecular chains. The significant decrease in the Raman band at approximately 100 cm^{-1} for the γ-PA6 sample at the same temperature range also supports this observation. Furthermore, it is evident that in α-PA6, an inflection of the band position at approximately 60 cm^{-1} occurs earlier than that at 100 cm^{-1} during the heating process, indicating that molecular rotation happens before the Brill transition point and plays a role in causing the rearrangement of hydrogen bonding and molecular chains.

The second derivative intensities at 100 cm^{-1} for both samples exhibited entirely different behaviors, as shown in Fig. 4(c). While the second derivative intensity of γ-PA6 generally decreased in absolute intensity, the second derivative intensity of α-PA6 remained stable until a significant inflection at 130 °C occurred, followed by a continuous decrease in absolute intensity. As the band is associated with the vibrating motion of backbone carbon atoms, the sudden broadening of the band suggests that the regularity of backbone carbon atom vibrations in α-PA6 starts to break down at approximately 130 °C, indicating the onset of molecular chain rotation. In contrast, due to weaker hydrogen bonding and greater molecular chain mobility, γ-PA6 displayed a continuous decline in the regularity of backbone carbon atom vibrations.

Fig. 4(d) shows a similar decrease in absolute second derivative intensities at 60 cm^{-1} for α-PA6, indicating a decline in the regularity of rotational motion of the backbone chains as the temperature increases and thermal motion intensifies; however, the rate of decrease slowed after the Brill transition

point, suggesting that the transition from a monoclinic to a pseudo-hexagonal structure may have increased the homogeneity of molecular chain rotation in the α-form. With the consistency between the results from quantum chemical calculations and the experimental Raman spectra, it may be possible to conclude that the newly discovered band at approximately 60 cm^{-1} is attributable to the local rotational motion of molecular chains. This may be the first time that this band has been clearly identified and assigned in experimental Raman spectral results.

For a supplementary understanding of low-wavenumber region results, the C–C stretching region in the high-frequency Raman spectra was a point of focus.

As shown in Fig. 5, the absolute intensity of the spectra in the high-wavenumber region decreased overall with increasing temperature for α- and γ-PA6, reaching a minimum near the Brill transition point and then increasing continuously. In addition, the relative heights of the characteristic peaks decreased with increasing temperature, reflecting a decrease in crystallinity.

The Raman shifts of the bands at approximately 1126, 1080, and 1060 cm^{-1} after Lorentzian fitting are shown in Fig. 6. As mentioned, these peaks are assigned to the *trans*, *gauche*, and *trans* conformations, respectively, aligning with the computational results. Obviously, the Raman shift of the vibrational modes from *trans* conformation in γ-PA6 was at a lower level compared with that of α-PA6. For the *gauche* band, however, the situation was reversed. These results are reasonable because the *trans* conformation is more common in the α-form while the *gauche* structure is characteristic of the γ-form crystal phase.[72]

During the heating process, Raman shifts of all three bands in both samples showed a mainly continuous redshift, indicating a weakening of the crystalline form; however, some details are worth noting: in α-PA6, the Raman shift of *trans* bands exhibited a slightly accelerated redshift rate after 130 °C. Conversely, the Raman shift of the *gauche* band ceased redshifting after 160 °C. These two inflections correspond with the behavior of the bands near 60 cm^{-1} and 100 cm^{-1} in the low-wavenumber region. This suggests that during the Brill transition in α-PA6, the rotation of the backbone disorders the *trans* conformation, leading to the rearrangement of hydrogen bonding and the formation of the *gauche* conformation.

In summary, based on the computational and experimental results, it was deduced that the gradual elongation of the lattice length and weakening of the hydrogen bonds with increasing temperature and the consequent increasing rotational mobility of the molecular chains against maintaining the *trans* conformation of the backbone are the reasons for the Brill transition in α-PA6. This transition leads to the rearrangement of molecular chains and hydrogen bonding.

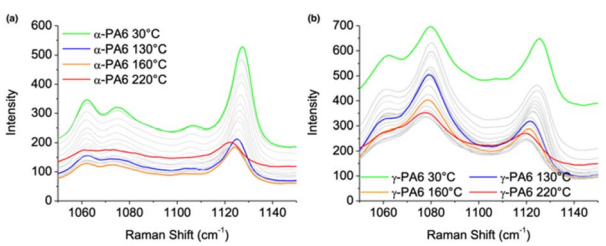

Fig. 5 Raman spectra in C–C stretching regions of (a) α-PA6 and (b) γ-PA6 as a function of temperature from 30 °C to 230 °C.

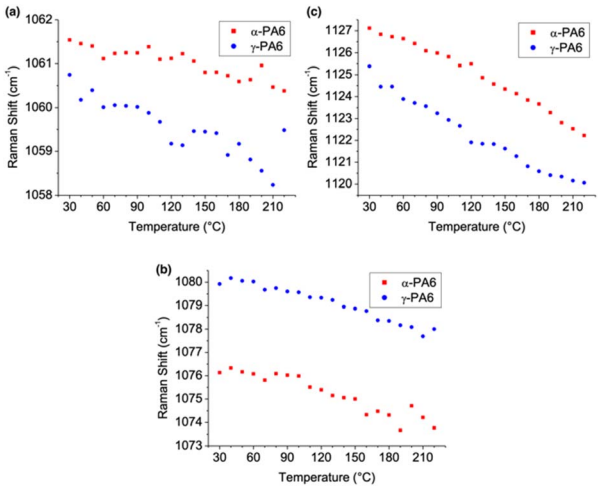

Fig. 6 Plots of the bands at approximately (a) 1060 cm^{-1}, (b) 1080 cm^{-1}, and (c) 1126 cm^{-1} as a function of temperature from 30 °C to 220 °C.

Conclusions

In this study, low-frequency Raman spectroscopy, along with quantum chemical calculations and high-frequency Raman spectroscopy, was used to investigate the Brill transition of PA6 with different crystal forms.

Quantum chemical calculations yielded results consistent with the experimental Raman spectra, providing clear assignments for the bands in the low- and high-wavenumber regions.

In the low-frequency Raman spectroscopy, a peak at approximately 100 cm^{-1} corresponds to the lateral motion of methylene groups and amide stretching, reflecting hydrogen bonding and lattice length. A newly identified peak at approximately 60 cm^{-1}, attributed to molecular chain torsions in the α-form, indicates that molecular chain rotation—triggered by increases in the lattice length—drives hydrogen bonding rearrangement during the Brill transition. To the best of our knowledge, this provides the first interpretation of the Brill transition mechanism in PA6 using low-frequency Raman techniques.

In the high-frequency Raman spectroscopy, the bands at approximately 1126, 1080, and 1060 cm^{-1} suggest that disordering of the *trans* conformation occurs because of backbone rotation, followed by *gauche* conformation formation during the Brill transition.

Compared with high-frequency Raman spectra, the low-frequency Raman spectra provided distinct and noticeable insights into the mechanism of Brill transition. The band at approximately 60 cm^{-1} was found exclusively in α-PA6, exhibited high sensitivity to the Brill transition, and offered direct

information regarding molecular chain rotation. The ability to detect low-energy vibrations such as hydrogen bond modes, crystal-lattice modes, and intermolecular modes,[73,74] demonstrates the great potential of low-frequency Raman spectroscopy for studying the crystalline properties of polymers.

Data availability

The data supporting this article have been included as part of the article or its ESI.†

Author contributions

Jiacheng Gao: formal analysis, investigation, and writing – original draft. Harumi Sato: supervision and writing – review and editing.

Conflicts of interest

There are no conflicts to declare.

Acknowledgements

This work was supported by JST SPRING, Grant Number JPMJSP2148.

References

1 M. Lewin, *Handbook of Fiber Chemistry*, CRC Press Boca Raton, 3rd edn, 2006.
2 H. Li, Y. Wu, H. Sato, L. Kong, C. Zhang, K. Huang, D. Tao, J. Chen, X. Liu, Y. Zhao, Y. Xu, J. Wu and Y. Ozaki, *Macromolecules*, 2009, **42**, 1175–1179.
3 C. Quarti, A. Milani, B. Civalleri, R. Orlando and C. Castiglioni, *J. Phys. Chem. B*, 2012, **116**, 8299–8311.
4 M. Romero-Fernandez, C. M. Heckmann and F. Paradisi, *ChemSusChem*, 2022, **15**, e202200811.
5 V. Miri, O. Persyn, J.-M. Lefebvre and R. Seguela, *Eur. Polym. J.*, 2009, **45**, 757–762.
6 M. Shakiba, E. Rezvani Ghomi, F. Khosravi, S. Jouybar, A. Bigham, M. Zare, M. Abdouss, R. Moaref and S. Ramakrishna, *Polym. Adv. Technol.*, 2021, **32**, 3368–3383.
7 P. Matthies and W. F. Seydl, High Performance Polymers: Their Origin and Development, in *History and Development of Nylon 6*, ed. R. B. Seymour and G. S. Kirshenbaum, Springer Dordrecht, Berlin, 1986, pp. 39–53.
8 M. Sudhakar, C. Priyadarshini, M. Doble, P. Sriyutha Murthy and R. Venkatesan, *Int. Biodeterior. Biodegrad.*, 2007, **60**, 144–151.
9 H. Suzuki, S. Ishii, C. Otani and H. Hoshina, *Eur. Polym. J.*, 2015, **67**, 284–291.
10 H. Suzuki, S. Ishii, H. Sato, S. Yamamoto, Y. Morisawa, Y. Ozaki, T. Uchiyama, C. Otani and H. Hoshina, *Chem. Phys. Lett.*, 2013, **575**, 36–39.
11 Y. Zhang, Y. Zhang, S. Liu, A. Huang, Z. Chi, J. Xu and J. Economy, *J. Appl. Polym. Sci.*, 2011, **120**, 1885–1891.
12 M. Musso, A. Reyer and D. Bertoldo Menezes, *Spectroscopy*, 2016, **31**, 44–48.
13 B. Lotz, *Macromolecules*, 2021, **54**, 565–583.
14 K. Tashiro and Y. Yoshioka, *Polymer*, 2004, **45**, 4337–4348.
15 J. Pepin, V. Miri and J.-M. Lefebvre, *Macromolecules*, 2016, **49**, 564–573.
16 J.-R. Xu, X.-K. Ren, T. Yang, X.-Q. Jiang, W.-Y. Chang, S. Yang, A. Stroeks and E.-Q. Chen, *Macromolecules*, 2018, **51**, 137–150.
17 H. Shanak, A. Naumann, J. Lion, W. Götz and R. Pelster, *J. Mater. Sci.*, 2014, **49**, 8074–8083.
18 N. Vasanthan and D. R. Salem, *J. Polym. Sci., Part B:Polym. Phys.*, 2000, **38**, 516–524.
19 K. Hedicke, H. Wittich, C. Mehler, F. Gruber and V. Altstädt, *Compos. Sci. Technol.*, 2006, **66**, 571–575.
20 M. A. Batistella, R. Sonnier, B. Otazaghine, C. O. Petter and J. M. Lopez-Cuesta, *Appl. Clay Sci.*, 2018, **157**, 248–256.
21 K. P. Pramoda, T. Liu, Z. Liu, C. He and H.-J. Sue, *Polym. Degrad. Stab.*, 2003, **81**, 47–56.
22 V. Fernández-González, J. M. Andrade, B. Ferreiro, P. López-Mahía and S. Muniategui-Lorenzo, *Spectroc. Acta Pt. A-Molec. Biomolec. Spectr.*, 2021, **263**, 120162.
23 T. X. Liu, Z. H. Liu, K. X. Ma, L. Shen, K. Y. Zeng and C. B. He, *Compos. Sci. Technol.*, 2003, **63**, 331–337.
24 P. Colomban and G. Gouadec, *Compos. Sci. Technol.*, 2009, **69**, 10–16.
25 H. Uematsu, T. Kawasaki, K. Koizumi, A. Yamaguchi, S. Sugihara, M. Yamane, K. Kawabe, Y. Ozaki and S. Tanoue, *Polymer*, 2021, **223**, 123711.
26 N. Abacha, M. Kubouchi and T. Sakai, *eXPRESS Polym. Lett.*, 2009, **3**, 245–255.
27 H. Shinzawa and J. Mizukado, *J. Mol. Struct.*, 2020, **1217**, 128389.
28 C. Jördens, S. Wietzke, M. Scheller and M. Koch, *Polym. Test.*, 2010, **29**, 209–215.
29 T. Lechner, K. Noack, M. Thöne, P. Amend, M. Schmidt and S. Will, *Phys. Procedia*, 2016, **83**, 1271–1278.
30 N. Vasanthan, N. S. Murthy and R. G. Bray, *Macromolecules*, 1998, **31**, 8433–8435.
31 D. Yan, Y. Li and X. Zhu, *Macromol. Rapid Commun.*, 2000, **21**, 1040–1043.
32 Y. Huang, W. Li and D. Yan, *Eur. Polym. J.*, 2003, **39**, 1133–1140.
33 Y. Yoshioka and K. Tashiro, *Polymer*, 2003, **44**, 7007–7019.
34 W. Li, Y. Huang, G. Zhang and D. Yan, *Polym. Int.*, 2003, **52**, 1905–1908.
35 C. Wang, S.-Y. Tsou and H.-S. Lin, *Colloid Polym. Sci.*, 2012, **290**, 1799–1809.
36 C.-Y. Ho, P.-H. Chen, C.-F. Yang, U.-S. Jeng and A.-C. Su, *ACS Appl. Polym. Mater.*, 2021, **3**, 1042–1051.
37 D. B. Menezes, A. Reyer and M. Musso, *Spectroc. Acta Pt. A-Molec. Biomolec. Spectr.*, 2018, **190**, 433–441.
38 S. Yamamoto, E. Ohnishi, H. Sato, H. Hoshina, D. Ishikawa and Y. Ozaki, *J. Phys. Chem. B*, 2019, **123**, 5368–5376.
39 Z. Xu, Z. He, Y. Song, X. Fu, M. Rommel, X. Luo, A. Hartmaier, J. Zhang and F. Fang, *Micromachines*, 2018, **9**, 361.

40 B. Schrader, *Angew Chem. Int. Ed. Engl.*, 1973, **12**, 884–908.
41 T. Vankeirsbilck, A. Vercauteren, W. Baeyens, G. Van der Weken, F. Verpoort, G. Vergote and J. P. Remon, *Trends Anal. Chem.*, 2002, **21**, 869–877.
42 G. P. S. Smith, G. S. Huff and K. C. Gordon, *Spectroscopy*, 2016, **31**, 42–50.
43 C. Nims, B. Cron, M. Wetherington, J. Macalady and J. Cosmidis, *Sci. Rep.*, 2019, **9**, 7971.
44 E. M. Paiva, R. L. Ribessi, C. Fernandes Pereira and J. J. Rodrigues Rohwedder, *Spectroc. Acta Pt. A-Molec. Biomolec. Spectr.*, 2020, **228**, 117798.
45 K. Takazawa, *J. Anal. Methods Chem.*, 2022, **2022**, 2694545.
46 S. Yamamoto, Y. Morisawa, H. Sato, H. Hoshina and Y. Ozaki, *J. Phys. Chem. B*, 2013, **117**, 2180–2187.
47 D. Marlina, H. Hoshina, Y. Ozaki and H. Sato, *Polymer*, 2019, **181**, 121790.
48 N. Ueno and H. Sato, *Spectroc. Acta Pt. A-Molec. Biomolec. Spectr.*, 2024, **312**, 124052.
49 S. Yamamoto, M. Miyada, H. Sato, H. Hoshina and Y. Ozaki, *J. Phys. Chem. B*, 2017, **121**, 1128–1138.
50 A. Nishimae and H. Sato, *Macromolecules*, 2021, **54**, 6440–6448.
51 T. Segawa, K. Ito, M. Hatayama, Y. Maruyama, J. Gao, N. Ueno and H. Sato, *ACS Appl. Polym. Mater.*, 2024, **6**, 6408–6415.
52 S. Tatsuoka and H. Sato, *Spectroc. Acta Pt. A-Molec. Biomolec. Spectr.*, 2018, **197**, 95–102.
53 Y. Yamamoto, H. Hoshina and H. Sato, *Macromolecules*, 2021, **54**, 1052–1062.
54 Y. Maruyama, K. Tamura, K. Akao, Y. Ozaki and H. Sato, *Macromolecules*, 2024, **57**, 5340–5349.
55 P. Simon and G. Argay, *J. Polym. Sci., Polym. Phys. Ed.*, 1978, **16**, 935–937.
56 N. A. Jones, P. Sikorski, E. D. T. Atkins and M. J. Hill, *Macromolecules*, 2000, **33**, 4146–4154.
57 M. J. Frisch, G. W. Trucks, H. B. Schlegel, G. E. Scuseria, M. A. Robb, J. R. Cheeseman, G. Scalmani, V. Barone, B. Mennucci, G. A. Petersson, H. Nakatsuji, M. Caricato, X. Li, H. P. Hratchian, A. F. Izmaylov, J. Bloino, G. Zheng, J. L. Sonnenberg, M. Hada, M. Ehara, K. Toyota, R. Fukuda, J. Hasegawa, M. Ishida, T. Nakajima, Y. Honda, O. Kitao, H. Nakai, T. Vreven, J. A. Montgomery, Jr., J. E. Peralta, F. Ogliaro, M. Bearpark, J. J. Heyd, E. Brothers, K. N. Kudin, V. N. Staroverov, R. Kobayashi, J. Normand, K. Raghavachari, A. Rendell, J. C. Burant, S. S. Iyengar, J. Tomasi, M. Cossi, N. Rega, J. M. Millam, M. Klene, J. E. Knox, J. B. Cross, V. Bakken, C. Adamo, J. Jaramillo, R. Gomperts, R. E. Stratmann, O. Yazyev, A. J. Austin, R. Cammi, C. Pomelli, J. W. Ochterski, R. L. Martin, K. Morokuma, V. G. Zakrzewski, G. A. Voth, P. Salvador, J. J. Dannenberg, S. Dapprich, A. D. Daniels, Ö. Farkas, J. B. Foresman, J. V. Ortiz, J. Cioslowski, and D. J. Fox, *Gaussian 09 (Revision D.01)*, Gaussian Inc., Wallingford CT, 2009.
58 P. Bouř, *Qgrad*, Academy of Sciences, Prague, 2006.
59 T. Yanai, D. P. Tew and N. C. Handy, *Chem. Phys. Lett.*, 2004, **393**, 51–57.
60 S. Grimme, S. Ehrlich and L. Goerigk, *J. Comput. Chem.*, 2011, **32**, 1456–1465.
61 P. Bouř, *CCT, Program for Cartesian Tensor Transfer*, Academy of Sciences, Prague, 2009.
62 M. D. Hanwell, D. E. Curtis, D. C. Lonie, T. Vandermeersch, E. Zurek and G. R. Hutchison, *J. Cheminf.*, 2012, **4**, 17.
63 K. Momma and F. Izumi, *J. Appl. Crystallogr.*, 2011, **44**, 1272–1276.
64 P. Bouř, *PLAY*, Academy of Sciences, Prague, 1995.
65 O. Faurskov Nielsen, D. H. Christensen and O. Have Rasmussen, *J. Mol. Struct.*, 1991, **242**, 273–282.
66 S. Brunsgaard Hansen, D. H. Christensen and O. Faurskov Nielsen, *Spectrochim. Acta*, 1993, **49A**, 769–774.
67 J. M. Herrera Ramirez, P. Colomban and A. Bunsell, *J. Raman Spectrosc.*, 2004, **35**, 1063–1072.
68 K. Song and J. F. Rabolt, *Macromolecules*, 2001, **34**, 1650–1654.
69 B. Morelli, *J. Pharm. Biomed. Anal.*, 1995, **13**, 219–227.
70 M. An, Q. Zhang, Y. Lin, D. Wang, W. Chen, L. Meng, P. Yin and L. Li, *Macromolecules*, 2020, **53**, 11153–11165.
71 J. Xia, S. Xu, Y. Zheng, J. Zhou, C. Yu, G. Shan, Y. Bao and P. Pan, *Macromolecules*, 2022, **55**, 6090–6101.
72 J. S. Stephens, D. B. Chase and J. F. Rabolt, *Macromolecules*, 2004, **37**, 877–881.
73 K. Ajito, Y. Ueno and H.-J. Song, *NTT Tech. Rev.*, 2012, **10**, 32–37.
74 M. Takahashi, *Crystals*, 2014, **4**, 74–103.